Monte Carlo simulations concerning modeling DC and high power pulsed magnetron sputtering for Ti_3SiC_2 including high pressures and ion deposition probabilities

Jürgen Geiser

Humboldt-Universität zu Berlin,
Department of Mathematics,
Unter den Linden 6, D-10099 Berlin, Germany
geiser@mathematik.hu-berlin.de

Abstract. We motivate our study by simulating the particle transport of a thin film deposition process done by PVD (physical vapor deposition) processes. In this paper we present a new model taken into account a higher pressure regimes in a sputter process. We propose a collision models for projectile and target collisions in order to compute the mean free path and include the virial coefficients that considered interacting gas particles.

A detailed description of collision models of the Monte Carlo Simulations is discussed for high power impulse magnetron sputtering (HIPIMS) and DC sputtering in lower pressure regimes.

We derive an equation for the mean free path for arbitrary interactions (cross sections) which (most important) includes the relative velocity between the projectiles and targets based on physical first principles and extend with higher order Virial terms .

At the substrate we simulate the implantation of the particles with the help of TRIM, based on result of the energy that are computed with the Monte Carlo methods.

We apply our results to three interaction models: hard sphere interaction, Screened Coulomb interaction and a mixture of the last mentioned interactions.

The deposition to realistic geometries, which have sharp angles included, are presented. Because of the strong convective process of a HIPIMS method, the low diffusion process allows not to deposit into delicate geometries, see [2]. This can be improved by rotating the target to a more or less perpendicular angle.

Keywords: High power pulsed magnetron sputtering, DC sputtering, Hard sphere interaction, Screened Coulomb, viral expansion, implantation model, Monte Carlo simulations.
AMS subject classifications. 78M31, 80M31,74A25.

1 Introduction

We motivate our studying on simulating a thin film deposition process that can be done with PVD (physical vapor deposition) processes or sputtering processes. In the last years, due to the research in producing high temperature films by depositing of low pressure processes have increased. The interest on standard applications to TiN and TiC are immense but recently also deposition with new material classes known as MAX-phases are important. The MAX-phase are nanolayered terniar metal-carbides or -nitrids, where M is a transition metal, A is an A-group element (e.g. Al, Ga, In, Si, etc.) and X is C (carbon) or N (nitrid).

In [7] we presented a model for low temperature and low pressure plasma. Here we extend our model to implantation and delicate geometries. While the implantation model allows to predict the penetration into the target material, the sputter angle to the target material is important to obtain at least the deposition with the particles.

The model is based on a simple pathway model, see [2], and we achieve with particle tracking the deposition rates. The stoichiometry is given as $3Ti$, Si and $2C$ and corresponds to the Max-phase material Ti_3SiC_2.

The paper is outlined as follows.

In section 2 we present our mathematical model and a possible reduced model for the further approximations. The numerical experiments and physical experiments are given in Section 3. In the contents, that are given in Section 4, we summarize our results.

2 Mathematical Model

In the following, the models of the particle transport in the apparatus are discussed in two directions:

1. Ideal Gas (non interacting and non overlapping gas particles, high vacuum)
2. Real Gas (interacting gas particles, lower pressure regimes)

The modeling is considered by the deriving the free path length with the so called Virial coefficients.

2.1 Ideal and Real Gases

The ideal gas is given by the ideal gas law:

$$pV = RT, \tag{1}$$

where p is the pressure, T the temperature, V is the volume and R is the gas constant.

It is the equation of state of a hypothetical ideal gas. It is a good approximation to the behavior of many gases under many conditions and has several limitations, e.g. higher pressures.

For the models we assume to high vacuum and non overlapping with particles.

To be more realistic we derive the so called virial expansion for the real gas, that is discussed in the statistical mechanics see [1].

Virial Expansion for Real Gases The virial expansion is written as

$$\frac{p}{K_B T} = \frac{N}{V} + B_2 \left(\frac{N}{V}\right)^2 + B_3 \left(\frac{N}{V}\right)^3 + ... \tag{2}$$

where the coefficients B_m are called the Virial coefficients and are in general functions of the gas temperature T. By neglecting higher order virial coefficients, one recognizes the equation of state of an ideal gas (non-interacting gas particles). Thus, the virial expansion may be regarded as a low-density approximation to the equation of state. The Virial coefficients for the hard-sphere interaction potential are calculated by several authors. Clisby and McCoy calculated in 2006 the ninth and tenth order Virial coefficient. The following table shows the Virial coefficients for the hard-sphere potential up to the tenth order. Whereby we made use of

$$b = B_2 = \frac{2}{3}\pi R^3, \tag{3}$$

with $R = (r_1 + r_2)$ the effective collision diameter.

B_2/b	1
B_3/b^2	0.625
B_4/b^3	0.2869495
B_5/b^4	0.110252
B_6/b^5	0.03888198
B_7/b^6	0.01302354
B_8/b^7	0.0041832
B_9/b^8	0.0013094
B_{10}/b^9	0.0004035

In order to incorporate the state equation of a real hard-sphere gas one is not interested in an expansion of the form

$$p = f(\frac{N}{V}) = f(\rho) = a_1\rho + a_2\rho^2 + a_3\rho^3 + ..., \tag{4}$$

but one needs the revers series

$$\rho = g(p) = A_1 p + A_2 p^2 + A_3 p^3 + ... \tag{5}$$

The series reversion can be done almost immediately By plugging (4) into (5), and the following equation is obtained

$$\rho = g(p) = (a_1 A_1)\, p + \left(a_2 A_1^2 + a_1 A_2\right) p^2 + \left(a_3 A_1^3 + 2a_2 A_1 A_2 + a_1 A_3\right) p^3 + ... \tag{6}$$

Coefficient comparison between the LHS and RHS of Equation (6) gives the unknown coefficients of the revers series. The following tables shows the results.

m	A_m
1	$\frac{1}{a_1}$
2	$-\frac{a_2}{a_1^3}$
3	$\frac{2a_2^2-a_1a_3}{a_1^5}$
4	$\frac{-5a_2^3+5a_1a_3a_2-a_1^2a_4}{a_1^7}$
5	$\frac{14a_2^4-21a_1a_3a_2^2+6a_1^2a_4a_2+3a_1^2a_3^2-a_1^3a_5}{a_1^9}$
$\vdots$	...

We therefore have the following relation of the gas density with respect to the gas pressure (up to third order) of the following form

$$\rho_{(3)} = \frac{1}{K_B T}\left\{p - \left(\frac{2/3\pi^4 R^6}{K_B T}\right)p^2 + \left(\frac{(1.375)(2/3)^2\pi^8 R^{12}}{(K_B T)^2}\right)p^3\right\} \tag{7}$$

An approximation for the mean free path is therefore given by

$$\lambda = \frac{1}{\sqrt{\left(1+\frac{M_{ion}}{M_{target}}\right)}}\frac{K_B T}{\pi D^2\left\{p - \left(\frac{2/3\pi^4 R^6}{K_B T}\right)p^2 + \left(\frac{(1.375)(2/3)^2\pi^8 R^{12}}{(K_B T)^2}\right)p^3\right\}} \tag{8}$$

2.2 Implantation Model

Based on the results of the Particle tracking in the apparatus, we obtain the stoichiometry and the energy that occurs at the substrate. Based on these results, we compute with the software package TRIM the implantation at the substrate.

If we assume a simple consideration of the rates in the reactor, In experiments it is show that particles with an energy of $E \approx 0.1eV$ rest at the surface, while particles with an energy about $E \approx 10eV$ and higher will implant to the substrate.

We are interested on considering the growth of thin films, so that low energies are important to leave the particles at the surface.

We assume a basic deposition process, in which a deposition (implantation) can occur or the ion is reflected at the surface of the substrate. We used the software package TRIM in order to obtain the reflexion probability at the surface. This probability depends on the substrate configuration, the implantation species as well as its energy and the angle of approach at the substrate. We modeled a pure Fe-substrate (5 mm thickness) and determined the reflexion probability. The deposition probability is therefore the complement of the reflexion probability. In the Fig. 1 one can see the deposition probabilities for the different deposition species. At energies below 2 eV the deposition probability is 1 and therefore all ions are deposited at the substrate. At energies higher than 2 eV there is a non-zero probability of reflexion and therefore the deposition probability is lower than one. It is clear from first principles that the deposition probability decrease with increasing angle of approach. The most sensitive

ion is Carbon. Because even for low energetic Carbon ions there is a non-zero probability of reflexion at the substrate surface. We used these results (i.e. the deposition probabilities) in our Monte-Carlo simulation in order to have a proper description at the substrate.

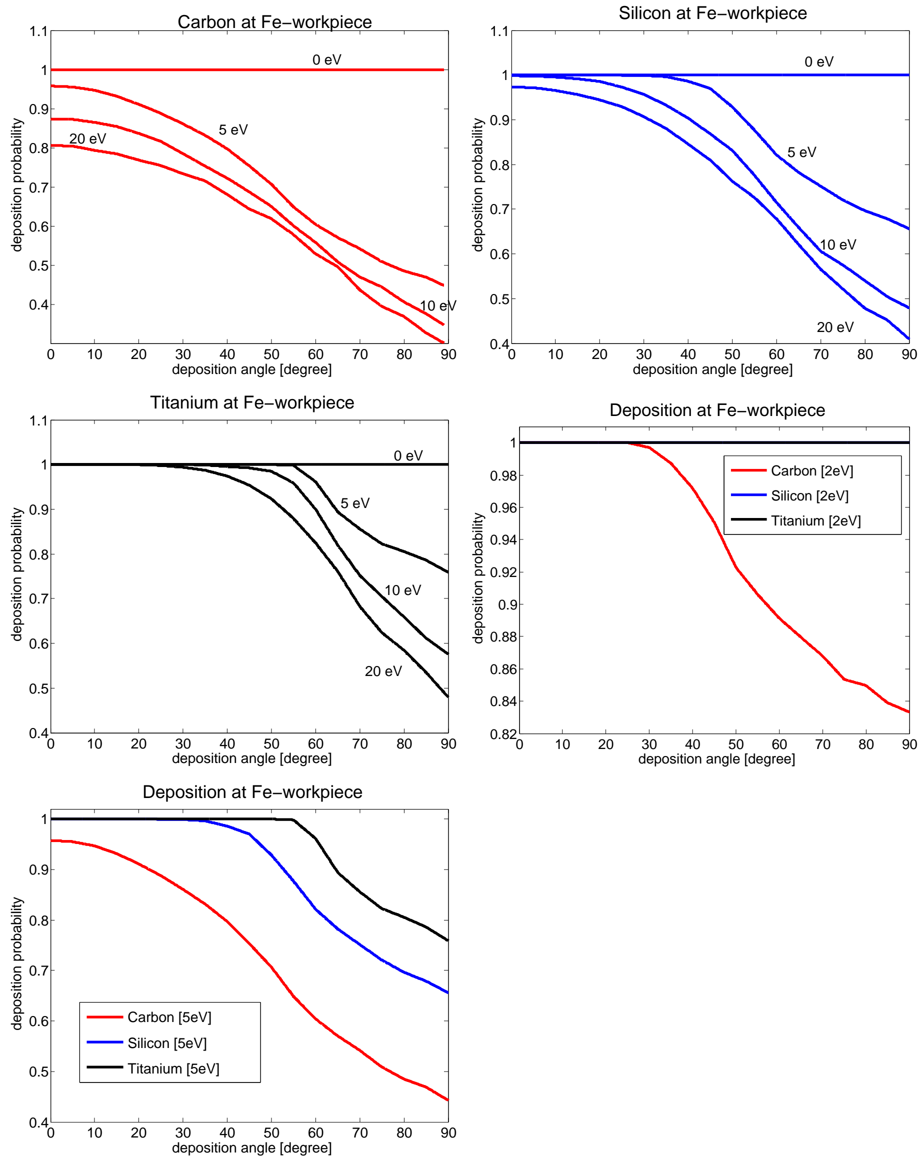

Fig. 1. Results from TRIM-Monte-Carlo simulations of ion implantation on Fe-substrate.
Deposition probability at specific energies with respect to the angle of substrate approach for **Upper left:** Carbon at Fe-substrate **upper right:** Silicon at Fe-substrate. **Middle left:** Titanium at Fe-substrate. As well as a direct comparison of the different deposition species **Middle right:** for impact energy of 2 eV and **Lower left:** impact energy of 5 eV.

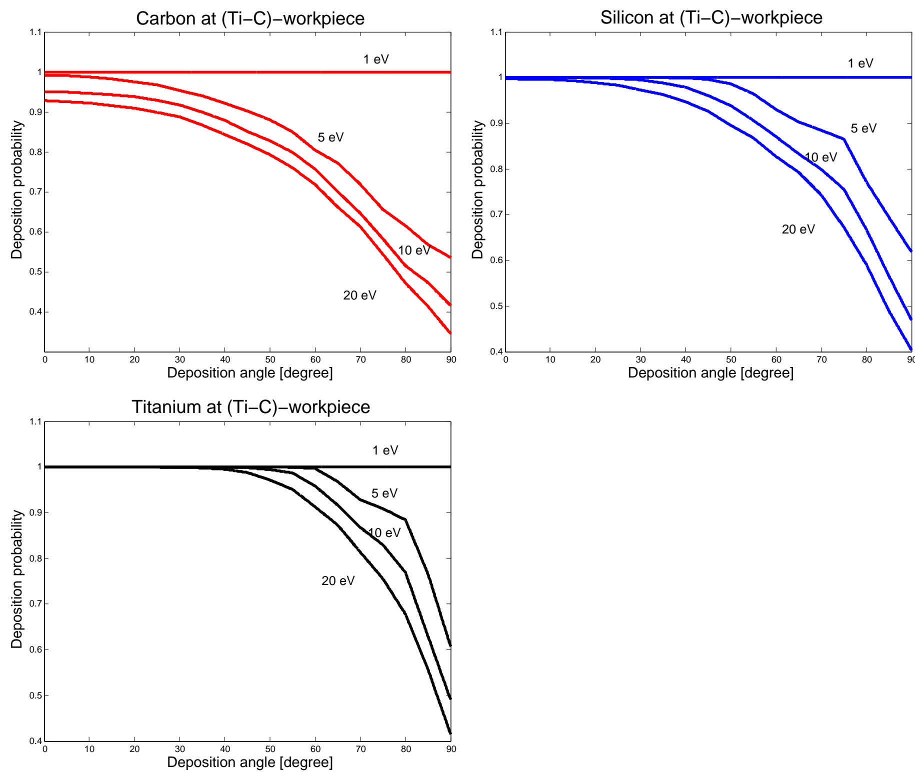

Fig. 2. Results from TRIM-Monte-Carlo simulations of ion implantation on Ti-C-substrate.
Deposition probability at specific energies with respect to the angle of substrate approach for **Upper left:** Carbon at Ti-C-substrate **upper right:** Silicon at Ti-C-substrate. **Middle left:** Titanium at Ti-C-substrate.

3 Monte Carlo simulations of the sputter process

In the following section we present the results from our analysis of the various sputter processes. In Table 1 one can see the configuration of our sputter reactor, whereby we used a Ti_3SiC_2-bulk sputter target (as we did in previous simulations). In Fig. 3 one can see our geometry of the simulated 2 dimensional sputter reactor.

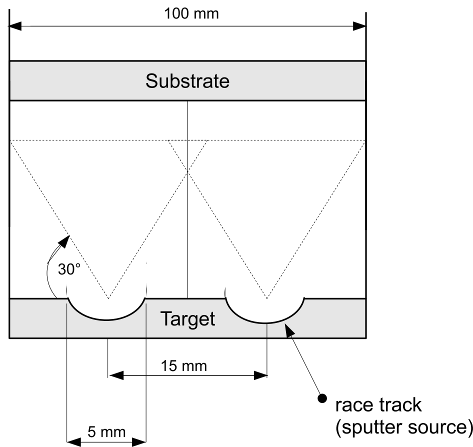

Fig. 3. Our chosen geometry of the simulated sputter reactor.

3.1 Sputtering from target

Sputtering from a circular planar magnetron causes the formation of a race-track in the target (see Fig. 3). The profile of the race-track is approximated by a Gauss distribution: $P(R) = \frac{1}{\sigma\sqrt{2\pi}} \exp\left(-\frac{R-\mu}{2\sigma^2}\right)$. The radius of the experimental race-track is 7.5mm (which is used for the mean μ of the gauss distribution) and the width of the race-track is 5 mm (from which the standard deviation is calculated to $3\sigma = 2.5$mm).

3.2 DC-Sputtering

We used the above mentioned implantation model based on TRIM and the experimental setup given in 1 in order to obtain the stoichiometric composition

Parameter	Value
Interaction-Type	pure hard sphere
Temperature (T)	300K
Ar-pressure (p_{Ar})	$1 \cdot 10^{-2}$mbar
S-T-distance (d)	constant 5 cm
Sputter target	bulk Ti_3SiC_2

Table 1. Experimental setup parameter concerning our sputter reactor.

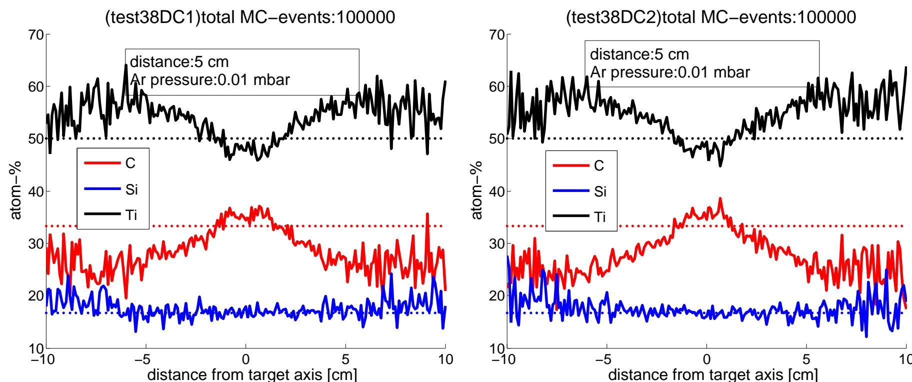

Fig. 4. Results from Monte-Carlo simulations of DC sputtering. Obtained stoichiometric decomposition at the substrate: **left:** with detailed deposition model and **right:** without detailed deposition model (no reflexion).

of our sputter reaction within the DC-mode. The results of our simulation can be see in Fig. 4

Experiments with higher MC-event with lower and higher deposition probability

In the next experiments, we tested the DC sputtering with higher deposition probability means, we taken into account the higher pressures, means a stronger diffusive process.

We compared standard MC-events (100000) and lower and higher deposition probability in Figure 5.

Remark 1. We have the following results to the experiments in Figure 5:

- Comparison standard simulations with 100000 events have the same results
- Higher or lower deposition probabilities at the substrate, did not change the results, because the mean free path is small comparing to the distance.
- Higher and lower pressure can only small influence the mean free path, so that we obtain the same deposition.
- All particles have energies smaller that $1eV$. Therefore the deposition probability is equal 1.

We can see from Trim simulations, that all particles deposit to the Fe substrate with $\leq 1eV$.

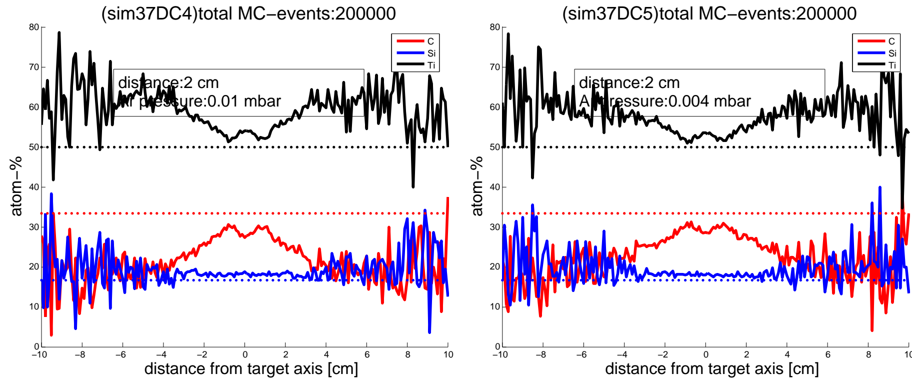

Fig. 5. Results from Monte-Carlo simulations of DC sputtering with 200000 events and different distances to the target.
Obtained stoichiometric decomposition at the substrate: **left:** with higher deposition probability and **right:** with lower deposition probability.

We compared standard MC-events (100000) and lower and higher deposition probability in Figure 5.

Remark 2. We have the following results to the experiments in Figure 6:

– Comparison with different distances to the target benefit the stoichiometry of the particles.
– Higher or lower deposition probabilities at the substrate, did not change the results, because the mean free path is also to small comparing to the distance.
– The control of the stoichiometry can be done with different distances.

3.3 HIPIMS-Sputtering

We used the above mentioned implantation model based on TRIM and the experimental setup given in 1 in order to obtain the stoichiometric composition of our sputter reaction within the HIPIMS-mode. Due to the fact that our Monte-Carlo algorithm is event-driven and not time driven, we model the effect of the HIPIMS-pulses with the help of a variable ionization degree of the background particles as well as the sputter species. Our approach is then as follows. The experimental effect of the high power pulses is that most of the background particles in the reactor a ionized within a pulse duration. The lower the pulse and the pulse duration the lower is the amount of ionized particles in the reactor. We model these effects by changing the ionization degree for some amount of sputtered particles. Our first approach is that 10 percent of the sputtered species are within a pulse. These particles see 70 percent of the background particles as ionized and therefore the interaction is a neutral-ion interaction or a ion-ion interaction depending on the ionization degree of the sputtered particle. In Table

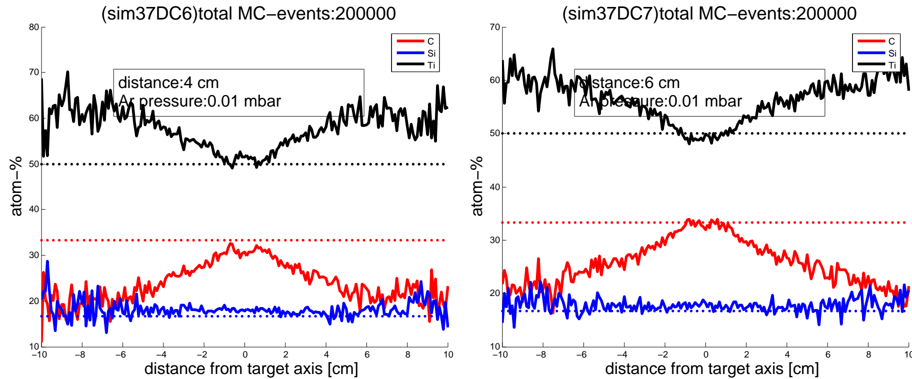

Fig. 6. Results from Monte-Carlo simulations of DC sputtering with 200000 events and different distances to the target.
Obtained stoichiometric decomposition at the substrate: **left:** with deposition probability ($4cm$ from target) and **right:** with deposition probability ($6cm$ from target).

2 one can see the basic assumptions about pulse duration and the ionization degree within and outside a HIPIMS pulse.

Parameter	Value
pulse width	10 %
Argon ionization (outside the pulse)	0%
Argon ionization (within the pulse)	70%
Carbon ionization (outside the pulse)	0%
Silicon ionization (outside the pulse)	0%
Titanium ionization (outside the pulse)	0%
Carbon ionization (within the pulse)	2%
Silicon ionization (within the pulse)	20%
Titanium ionization (within the pulse)	40%

Table 2. Experimental setup parameter concerning the HIPIMS simulation.

Based on the HIPIMS configuration given in Table 2 we performed a Monte-Carlo simulation (including the deposition model). The results can be seen in Fig. 7

3.4 Delicate deposition geometries

It is known that PVD processes and especially HIPIMS processes have problems to deposit into sharp angles (delicate geometries), see also the characterization in [**?**].

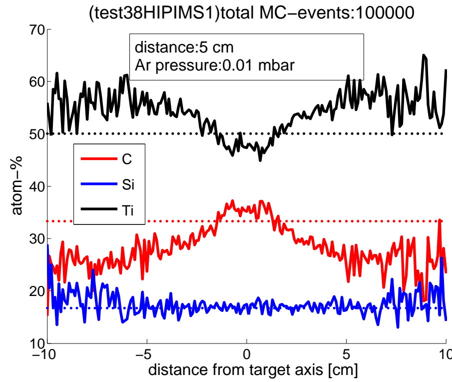

Fig. 7. Results from Monte-Carlo simulations of HIPIMS sputtering. Obtained stoichiometric decomposition at the substrate with detailed deposition model.

Based on a weak diffusive component, while sputting in a perpendicular angle from target to substrate, delicate geometries are hardy to deposit without rotating the substrate to the target in a perpendicular angle.

In the following we study to get diffusive effects with the PVD processes, e.g. to obtain deposition angles of the species of less than 90°.

- Higher pressure regimes to achieve more collisions and track into less than 90° angles
- larger distances from the target to achieve more collisions

Based on such modification, we can help to have a more diffusive behavior of the process.

Improved geometries are studied, see [6]

Geometry of Outlets

Perpendicular
and non−hidden
outlets ($\alpha < 90^{o}$)

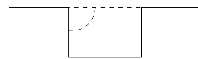

Obtuse
and hidden
outlets ($\alpha > 90^{o}$)

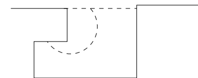

The simulation with Monte-Carlo methods are done in the following geometries:

The substrate can be rotated and we apply an extreme substrate as benchmark.

The parameterization is done in arc length.

So that we obtain a planar substrate to the coordinate x.

The sputter sources are given in $(x, y) = (-1, 0)$ and $(1, 0)$ and we can also combine various point sources.

In the figure 8 we obtain the amount of deposition rates to the delicate geometry. We see that nearly no deposition is obtained in sharp outlets.

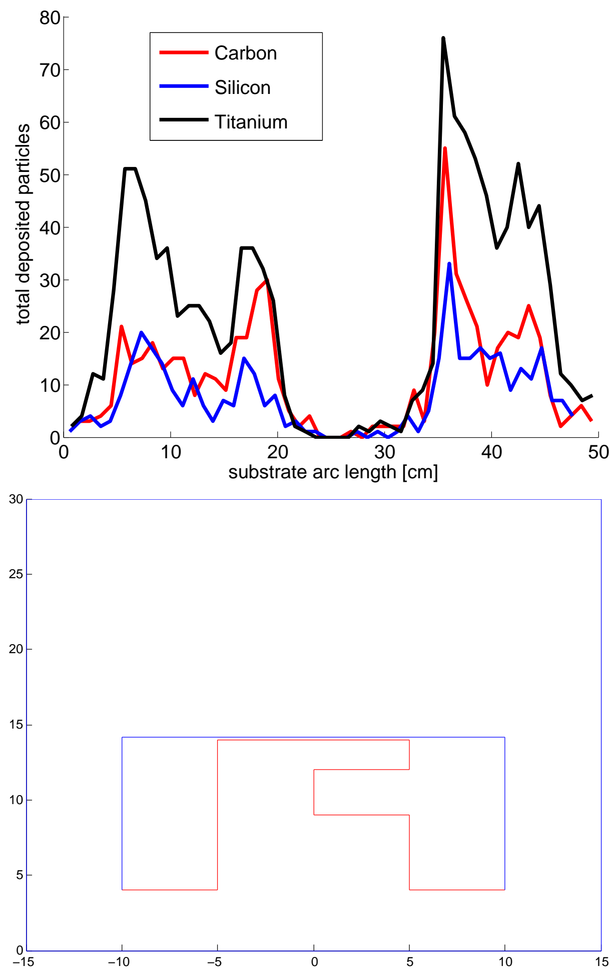

Fig. 8. Test geometry for the Monte-Carlo simulations of HIPIMS sputtering.

In the figure 9 we obtain the amount of deposition rates to the delicate and rotated geometry. We see that nearly no deposition is obtained in sharp outlets. We can increase small amount of the rates if we are perpendicular to the source.

Remark 3. Based on the low diffusive process of the HIPIMS and DC sputtering, it is impossible to deposit into geometries with obtuse angles or hidden areas. Such possibilities are given with CVD processes. By the way the idea is to rotate the target and have perpendicular deposition angles.

4 Conclusions and Discussions

We have extended our basic Monte-Carlo simulation model of Physical Vapor Deposition processes, see [7], with implantation and higher pressure regimes. We include the effects of higher background pressures and most important a realistic description of ion implantation at the substrate. Our results are in agreement with experimental dates. To control the deposition process, the variation of the point sources between source and target is a main benefit. Higher pressure regimes with longer distances can also improve the stoichiometry. In future, the ideal combination between various point and line sources can optimize the deposition or an additive diffusion, that can be done in a CVD (chemical vapor deposition) process.

Appendix

Scattering from a Screened Coulomb Potential (ion-ion interaction)

A classical description of scattering from a Screened Coulomb Potential leads to an infinite cross-section. However, a quantum mechanically approach gives within the Born approximation finite results. The screened Coulomb potential is given by

$$V(r) = \frac{Z_1 Z_2 k}{r} \exp -r/a \tag{9}$$

Whereby Z_1 and Z_2 are the atomic numbers of the collision partners, r is the radial distance between both partners, k is a constant ($k = 1.44$MeV fm) and a is the screening length given by

$$a = \frac{a_0}{\sqrt{\left(\sqrt{Z_1} + \sqrt{Z_2}\right)}}. \tag{10}$$

With $a_0 = 0.53 \cdot 10^{-10} m$ the first Bohr radius of the hydrogen atom. Within the frame work of Quantum Mechanics (Born approximation) the differential cross-section is given by the Fourier transform of the interaction potential $\widetilde{V}(\boldsymbol{\Delta})$, i.e.

$$\frac{d\sigma}{d\Omega} = \frac{\mu^2}{4\pi^2\hbar^4} \left|\widetilde{V}(\boldsymbol{\Delta})\right|^2 \tag{11}$$

The Fourier transform of our Screened Coulomb potential is given by

$$\widetilde{V}(\boldsymbol{\Delta}) = \frac{4\pi Z_1 Z_2 k}{\frac{1}{a^2} + \Delta^2} \tag{12}$$

The differential cross section is therefore given by

$$\frac{d\sigma}{d\Omega} = \left| \frac{Z_1 Z_2 k}{\frac{\hbar^2}{2\mu a^2} + 4E \sin^2(\theta/2)} \right|^2 . \tag{13}$$

Because of the Screening the differential cross section is always finite. The classical limit ($\hbar \to 0$) gives the divergent Rutherford cross section. If the differential cross section is of the following form:

$$\frac{d\sigma}{d\Omega} = \left(\frac{A}{B + C \sin^2(\theta/2)} \right)^2 , \tag{14}$$

and scattering events with scattering angles below a threshold value of θ_{min} can be neglected, then the total cross section is given by:

$$\sigma_{total} = \frac{2A^2\pi \left(\cos(\theta_{min}) + 1\right)}{(B + 4C)\left(B + 2C - 2C\cos(\theta_{min})\right)} \tag{15}$$

Hence the scattering angle probability distribution $P_{ScreenedCoulomb}(\theta)$ is given by

$$P_{ScreenedCoulomb}(\theta) = \frac{(B + 4C)(B + 2C - 2C\cos(\theta_{min}))\sin(\theta)}{(B + 2C - 2C\cos(\theta))^2(\cos(\theta_{min}) + 1)} \tag{16}$$

References

1. D. Chandler. *Introduction to Modern Statistical Mechanics.* Oxford University Press, 1987.
2. D.J. Christie. *Target material pathways model for high power pulsed magnetron sputtering.* J.Vac.Sci. Technology, 23:2, 330-335, 2005.
3. J. Geiser. *Numerical Simulation of a Model for Transport and Reaction of Radionuclides.* Proceedings of the Large Scale Scientific Computations of Engineering and Environmental Problems, Sozopol, Bulgaria, 2001.
4. J. Geiser. *Discretization methods with analytical solutions for convection-diffusion-dispersion-reaction-equations and applications.* Journal of Engineering Mathematics, published online, Oktober 2006.
5. J. Geiser. *Discretisation and Solver Methods with Analytical Methods for Advection-Diffusion-reaction Equations and 2D Applications.* Journal of Porous Media, Begell House Inc., Redding, USA, accepted March, 2008.
6. J. Geiser, V. Buck and M. Arab. *Model of PE-CVD apparatus: Verification and Simulations.* Mathematical Problems in Engineering, Hindawi Publishing Corp., New York, accepted, April 2010.

7. J. Geiser and S. Blankenburg. *Monte Carlo simulations concerning elastic scattering with application to DC and high power pulsed magnetron sputtering for Ti3 Si C2.* Preprint 2009-20, Humboldt University of Berlin, Department of Mathematics, Germany, 2009.
8. M.K. Gobbert and C.A. Ringhofer. *An asymptotic analysis for a model of chemical vapor deposition on a microstructured surface.* SIAM Journal on Applied Mathematics, 58, 737–752, 1998.
9. H.H. Lee. *Fundamentals of Microelectronics Processing* McGraw-Hill, New York, 1990.
10. S. Middleman and A.K. Hochberg. *Process Engineering Analysis in Semiconductor Device Fabrication* McGraw-Hill, New York, 1993.
11. M. Ohring. *Materials Science of Thin Films.* Academic Press, San Diego, New York, Boston, London, Second edition, 2002.
12. T.K. Senega and R.P. Brinkmann. *A multi-component transport model for non-equilibrium low-temperature low-pressure plasmas.* J. Phys. D: Appl.Phys., 39, 1606–1618, 2006.

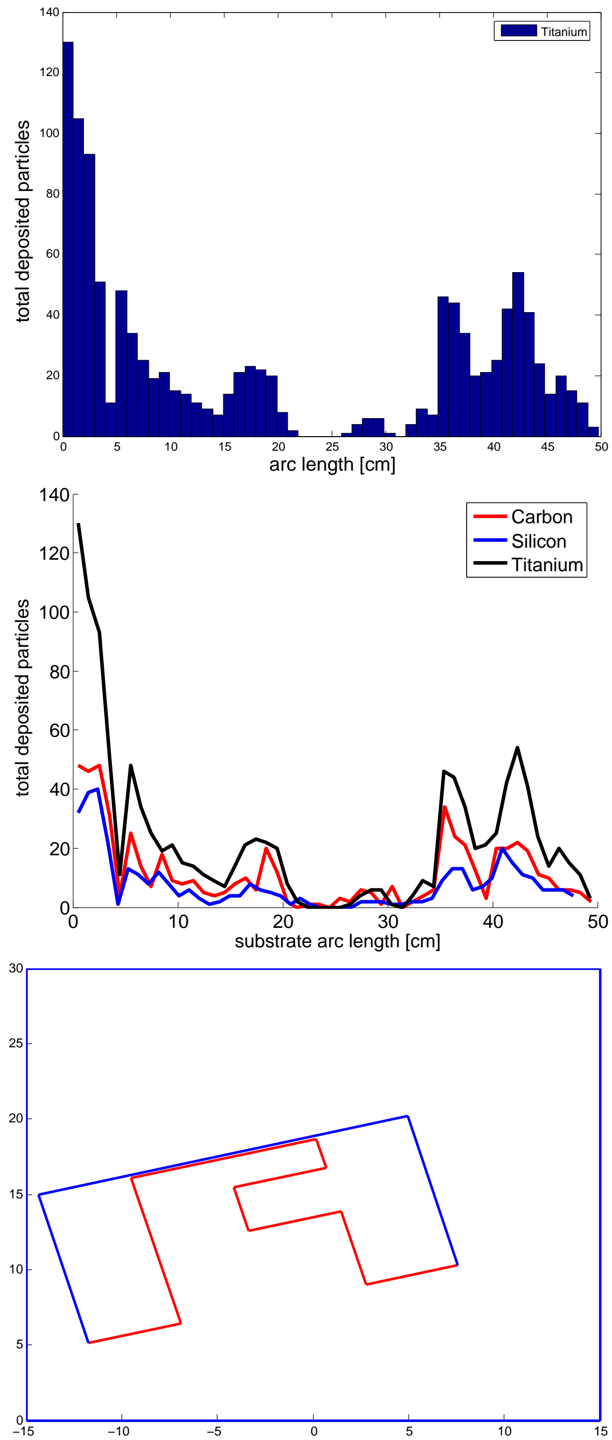

Fig. 9. Rotated test geometry for the Monte-Carlo simulations of HIPIMS sputtering.